

# Effect of BaTiO<sub>3</sub> on the microstructure and mechanical properties of Sn1.0Ag0.5Cu lead-free solder

Li Yang · Jinguo Ge · Yaocheng Zhang ·  
Jun Dai · Yanfeng Jing

Received: 28 September 2014 / Accepted: 23 October 2014 / Published online: 21 November 2014  
© Springer Science+Business Media New York 2014

**Abstract** Minor weight fraction of the BaTiO<sub>3</sub> particle is doped into the Sn1.0Ag0.5Cu (SAC) lead-free solder by the mechanically mixing. The effect of BaTiO<sub>3</sub> on the microstructure and mechanical properties of the SAC lead-free solder is investigated. The results show that the β-Sn is refined and the volume fraction of the eutectic phase is increased by adding BaTiO<sub>3</sub>. The β-Sn morphology is transformed from the block into the lamellar in the SAC + 0.2 wt% BaTiO<sub>3</sub>, and a Cu<sub>6</sub>Sn<sub>5</sub> IMC layer with thickness of about 7.3 μm is obtained. The optimal spreadability of the SAC–0.2BaTiO<sub>3</sub> is obtained, and the spreading coefficient reaches 0.7836, it is 23.48 % higher than that of the SAC solder. The ultimate tensile strength and the elongation are improved by the BaTiO<sub>3</sub> addition. The fracture surface of the SAC–0.2BaTiO<sub>3</sub> solder specimen consists of large amounts of dimples due to the highly ductile manner.

## 1 Introduction

The electronic devices are evolved to become light, small, and more functional with the rapid development of the

electronics industries, which require micro-joints to adapt to the harsh environment [1]. The SnPb solder with the superior performance was widely applied in the electronics industries in the past. Extensive efforts have been made to develop the suitable lead-free solders as substitution of the SnPb solder due to the realization of the health and environmental protection regarding the inherent toxicity of Pb [2, 3]. In the lead-free solder family, the SnAgCu eutectic solder is becoming one of the most popular solders to substitute the conventional SnPb solder due to the superior mechanical properties and high reliabilities [4, 5].

Several types of the ternary SnAgCu solders have been developed, including Sn3.9Ag0.6Cu (United States proposed), Sn3.8Ag0.7Cu (European Union proposed) and Sn3.0Ag0.5Cu (Japan proposed). The Ag content in the above SnAgCu solders is more than 3 wt%. The following three attempts have been adopted to modify the properties of the SnAgCu solder and reduce the cost. The first and most direct approach is to reduce the Ag content in the high-Ag lead free solders, the high-Ag solder can bring about a worse resistance to drop failure in the interconnections due to the formation of the thicker brittle Ag<sub>3</sub>Sn IMC layer in the soldering process. The strength phases are precipitated by adding the alloying elements to react with the original substrate solder and reduce the cost of the lead-free solder. El-Daly et al. [6] synthesized the quaternary Sn–Ag–Cu–Ni solder and the improved mechanical properties were obtained. Zhang et al. [7] found that the mechanical properties of SnAgCu lead-free solder were improved and the microstructure was refined by adding the small amount of Zn into the SnAgCu. Finally, some works reveal that a trace amount of enhanced particle are also the potentially feasible elements to modify the properties of the SnAgCu solder. Liu et al. [8] reported that the wetting property and the thermal expansion coefficient was improved by adding the graphene nanosheets into SnAgCu solder. Tsao and

---

L. Yang (✉) · J. Ge · Y. Zhang · J. Dai · Y. Jing  
School of Mechanical Engineering, Changshu Institute of  
Technology, Changshu 215500, Jiangsu, People's Republic of  
China  
e-mail: yangli2011@cslg.cn

L. Yang  
Jiangsu Key Laboratory of Large Engineering Equipment  
Detection and Control, Xuzhou Institute of Technology,  
Xuzhou 221008, Jiangsu, People's Republic of China

J. Ge · Y. Jing  
School of Materials Science and Engineering, China University  
of Mining and Technology, Xuzhou 221008, Jiangsu, People's  
Republic of China

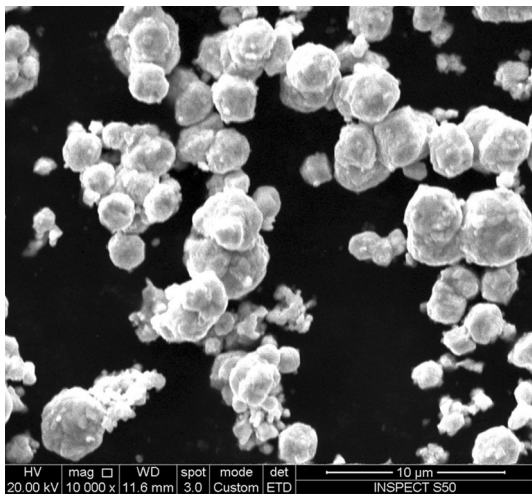


**Fig. 1** Morphology of the BaTiO<sub>3</sub> particle

Chang [9] reduced the grain size of  $\beta$ -Sn and Ag<sub>3</sub>Sn phase located between the spacing lamellae by TiO<sub>2</sub> addition. Some other alloying elements were also doped into the SAC solders to refine the microstructure and improve the mechanical properties, such as Sb [10], Co [11], In [12] and Bi [13] etc.

In the paper, the novel SAC–BaTiO<sub>3</sub> composite solders were fabricated by the mechanical mixing. The microstructure was examined by the optical microscope (OM) and the scanning electron microscopy (SEM) under back scatter electron pattern (BSED). The chemical composition of the intermetallic compounds (IMC) layer was inspected by the energy dispersive spectroscopy (EDS). The spreading coefficient was adopted to evaluate the spreadability. The ultimate tensile strength (UTS) and the elongation were carried out using the homemade micro mechanical test apparatus.

## 2 Experimental procedures

### 2.1 Materials and fabrication

The SAC solder with the size of about 45  $\mu$ m was used as the matrix alloy. The BaTiO<sub>3</sub> particle (99.99 % purity) with an average diameter of 3  $\mu$ m was added into the SAC solder. The morphology of the BaTiO<sub>3</sub> particle is shown in Fig. 1. The SAC–BaTiO<sub>3</sub> composite solders were fabricated in an airtight container using a roller blender with the rotate speed of 200 rpm for 1 h. The fabricated composite solders deposited in the gap of two copper sheets were heated at 280  $^{\circ}$ C for 5 min in the reflow furnace on the 5 mm thickness Al plate and then was air-cooled to the ambient temperature in the atmospheric environment. The nominal chemical composition of the four SAC–BaTiO<sub>3</sub> composite solder samples is listed in Table 1.

**Table 1** Nominal chemical composition of the fabricated composite solders (wt%)

Alloy	Ag	Cu	BaTiO <sub>3</sub>	Sn
SAC	1.0	0.5	0	Bal.
SAC–0.1BaTiO <sub>3</sub>	1.0	0.5	0.1	Bal.
SAC–0.2BaTiO <sub>3</sub>	1.0	0.5	0.2	Bal.
SAC–0.3BaTiO <sub>3</sub>	1.0	0.5	0.3	Bal.
SAC–0.4BaTiO <sub>3</sub>	1.0	0.5	0.4	Bal.

### 2.2 Spreadability measurement

The spreading coefficient was obtained by the following equation to evaluate the spreadability of the solders according to Japanese Industrial Standard JIS-Z3198-3:

$$K = \frac{D - H}{D} \quad (1)$$

where  $K$  is the spreading coefficient,  $D$  (mm) is the diameter of SAC ball,  $D = 1.24V^{1/3}$ ,  $V$  is the volume of the lead-free solder, and  $H$  (mm) is the maximum height of the solder alloy spreaded on the copper sheet.

### 2.3 Microstructural characterization

The SAC–BaTiO<sub>3</sub> samples were prepared by the standard metallographic procedures and the specimens were etched with a solution of 2 vol% HCl and 98 vol% alcohol. The microstructure was observed by the OLYMPUS PMG3 OM. The morphology of IMC layer and the chemical composition of the IMC layer were investigated by the INSPECTS50 SEM equipped with an EDS under BSED. The average thickness of the IMC layers was calculated by the following equation [14]:

$$T = \frac{\sum_{i=1}^n t_i}{n} \quad (2)$$

where  $t_i$  is the thickness of IMC layer at different positions on the interface,  $n$  is the number of the measurement,  $T$  is the average thickness of the IMC layer.

### 2.4 Tensile test

The dimension of the specimens for the tensile test is shown in Fig. 2. The specimens were annealed at 110  $^{\circ}$ C

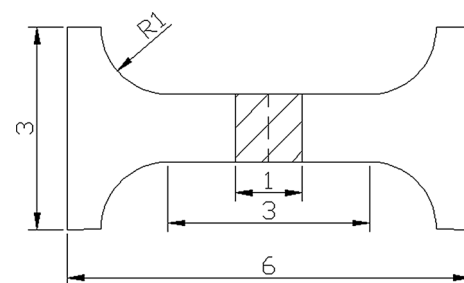


**Fig. 2** Schematically diagram showing the tensile specimen geometry

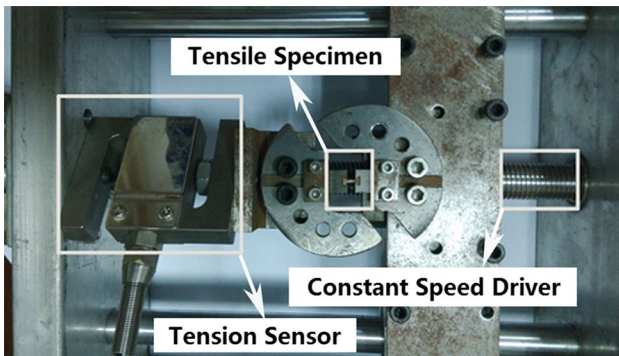


**Fig. 3** Homemade tensile testing machine

for 1 h, and then were air cooled to the room temperature. The tensile test was carried out using the homemade micro mechanical test apparatus with the tensile rate of 0.01 mm/s

[15], as shown in Fig. 3. Each experiment condition was evaluated as the average of three replicate tests for each solder. The fracture surfaces of specimens after tensile tests were observed by SEM.

### 3 Results and discussion

#### 3.1 Microstructure

Figure 4 presents the microstructure of the SAC and SAC–BaTiO<sub>3</sub> solders. As shown in Fig. 4a, the gray region in the SAC solder is the primary  $\beta$ -Sn phase, the dark region is the Ag<sub>3</sub>Sn + Cu<sub>6</sub>Sn<sub>5</sub> eutectic phase [16]. The primary  $\beta$ -Sn phase is refined and the volume fraction of the eutectic phase is increased by the addition of minor weight

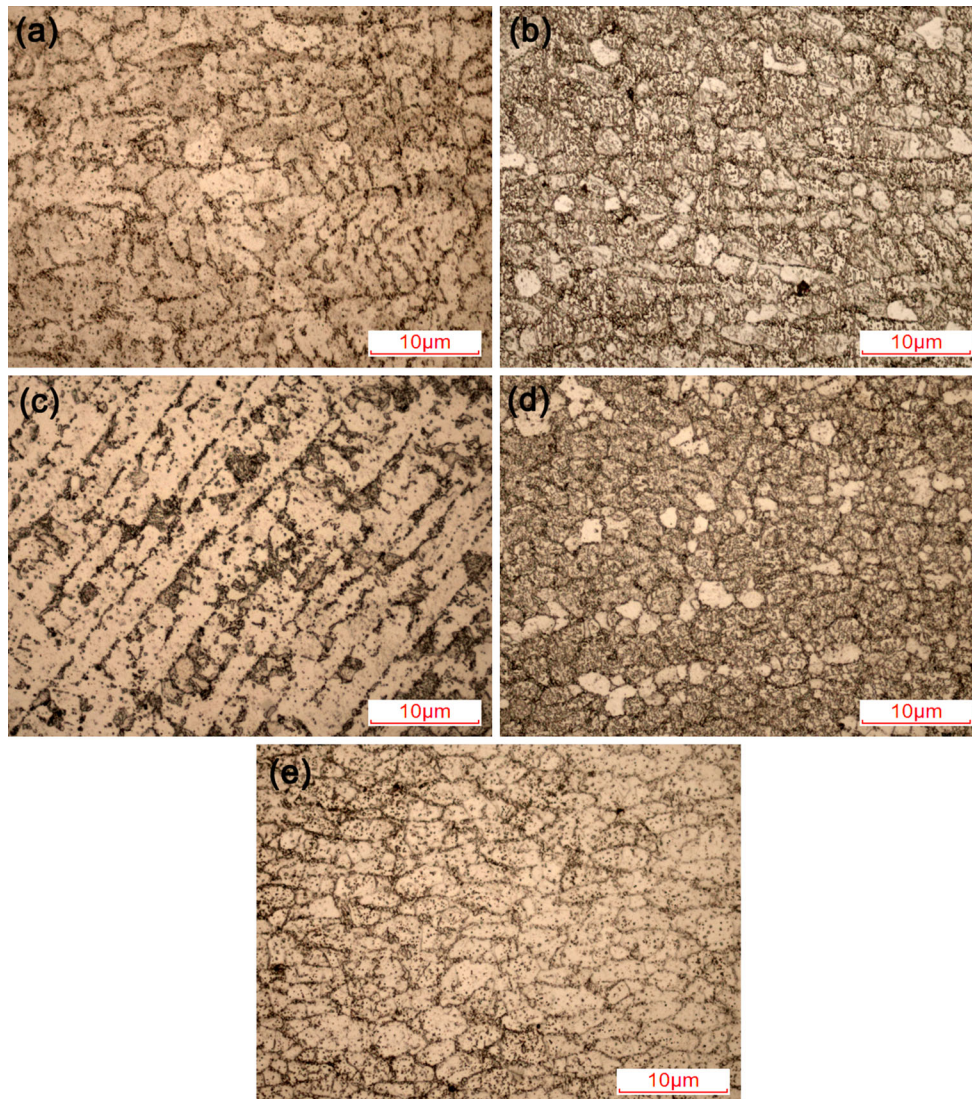


**Fig. 4** OM images of SAC and SAC–BaTiO<sub>3</sub> microstructure **a** SAC, **b** SAC–0.1BaTiO<sub>3</sub>, **c** SAC–0.2BaTiO<sub>3</sub>, **d** SAC–0.3BaTiO<sub>3</sub> and **e** SAC–0.4BaTiO<sub>3</sub>

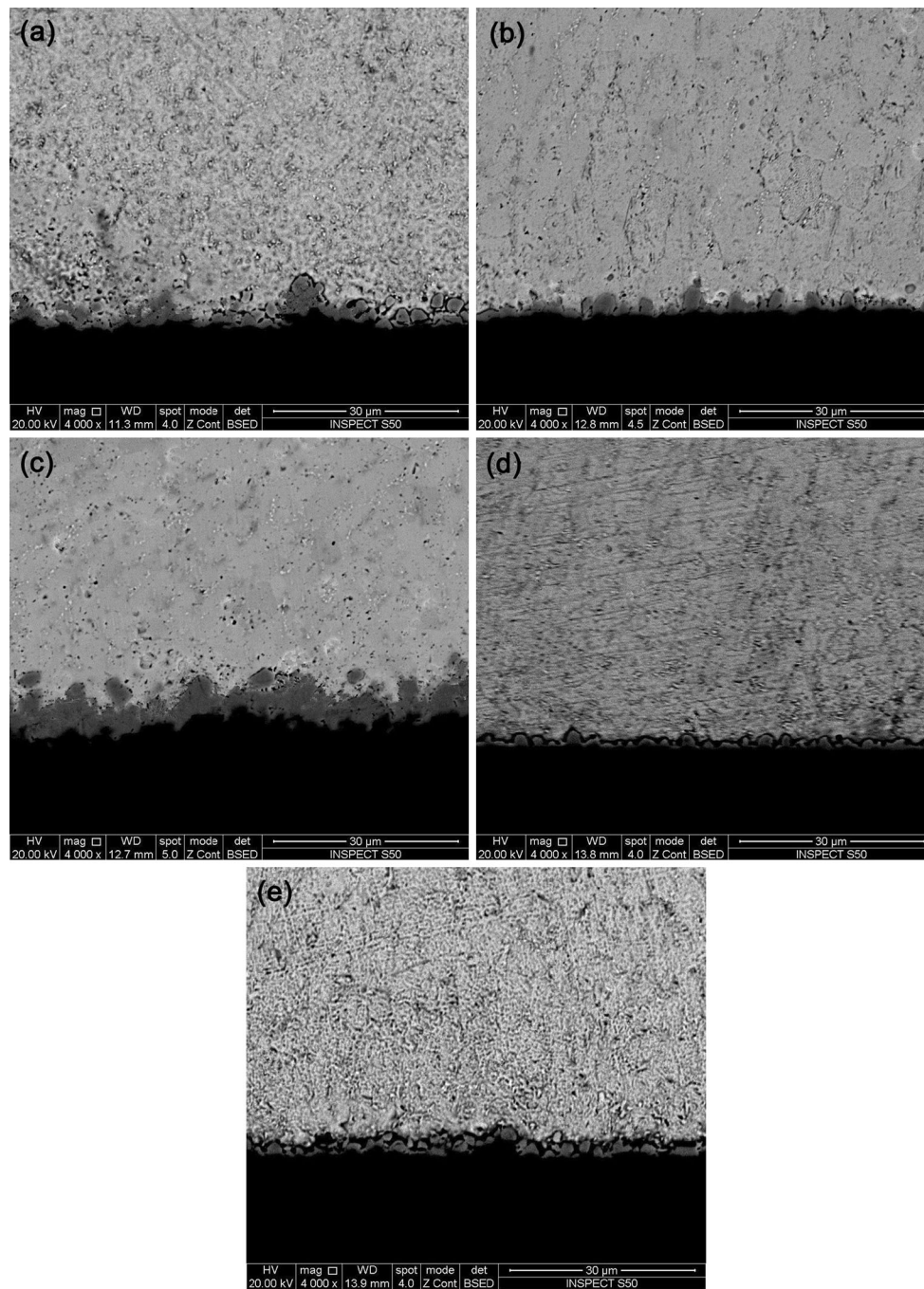


**Fig. 5** SEM images of SAC and SAC–BaTiO<sub>3</sub>, microstructure **a** SAC, **b** SAC–0.1BaTiO<sub>3</sub>, **c** SAC–0.2BaTiO<sub>3</sub>, **d** SAC–0.3BaTiO<sub>3</sub> and **e** SAC–0.4BaTiO<sub>3</sub>

of BaTiO<sub>3</sub>, as shown in Fig. 4b–e. The results can be explained by the theory of heterogeneous nucleation [2, 17], the primary  $\beta$ -Sn phase nucleates adherent to the surface of the BaTiO<sub>3</sub> particle, and then the formed primary  $\beta$ -Sn phase is served as the nucleation substance again during solidification. Hence, the corresponding size of the  $\beta$ -Sn phase is refined by the BaTiO<sub>3</sub> addition. In the Fig. 4c, the refined lamellar microstructure occurs in the

SAC–0.2BaTiO<sub>3</sub> solder. The coarsened block phase is not formed due to the degree of supercooling [18], the heat perpendicular to the copper sheets is lost quickly due to the appropriate thickness IMC layer formed firstly in the liquid solder, as shown in Fig. 5.

As illustrated in the Fig. 5, the IMC layer generated between the solder and the copper substrate, the scallop-shaped IMC layer is observed in the SAC–BaTiO<sub>3</sub> composite

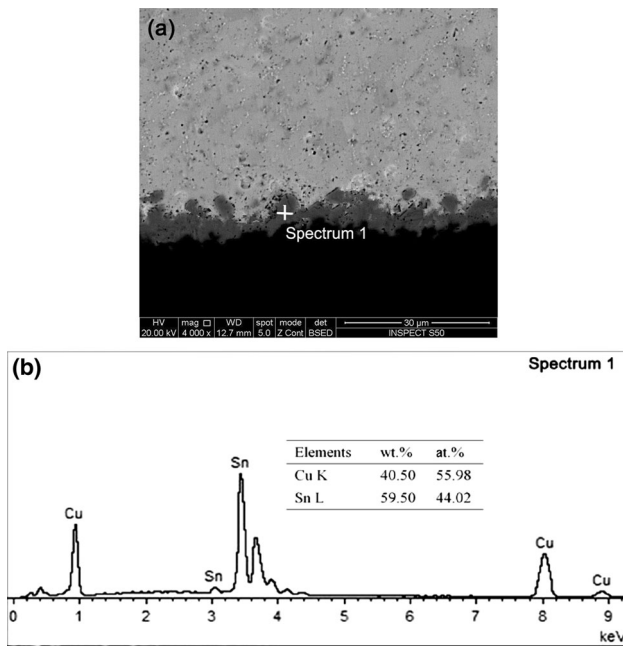


**Fig. 6** SEM micrographs of **a** SAC–0.2BaTiO<sub>3</sub> and **b** EDS analysis of the IMC layer in **a**

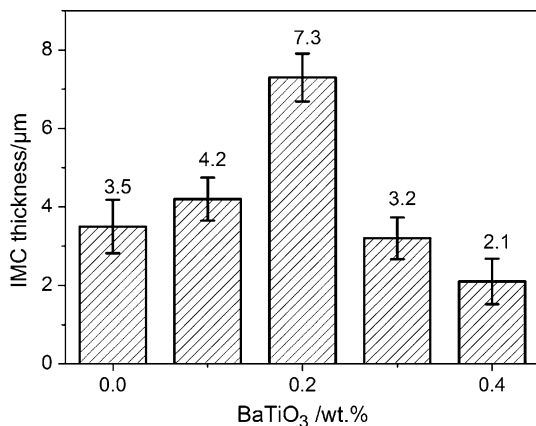


**Fig. 7** IMC layer thickness of SAC composite solders as a function of BaTiO<sub>3</sub> content

solders. Figure 6 shows the SEM image of the SAC–0.2BaTiO<sub>3</sub> composite solder and the corresponding EDS analysis. The chemical composition of the inspected IMC layer consists of 55.98 at.% Cu and 44.02 at.% Sn, and it is induced that the IMC is Cu<sub>6</sub>Sn<sub>5</sub>. The IMC thickness as a function of the content of BaTiO<sub>3</sub> particle is characterized in Fig. 7. The thickness is raised with increasing the BaTiO<sub>3</sub> content in the SAC–(0–0.2)BaTiO<sub>3</sub> composite solders, and the thickness of the SAC–0.2BaTiO<sub>3</sub> composite solder reaches about 7.3 μm that is twice thicker than that of the SAC solder.

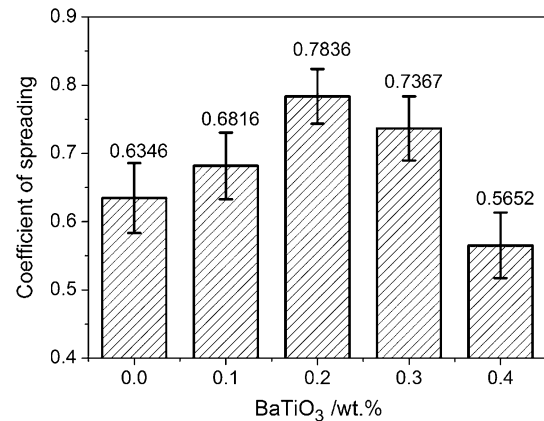


**Fig. 8** Effect of BaTiO<sub>3</sub> particle additions on spreading coefficient

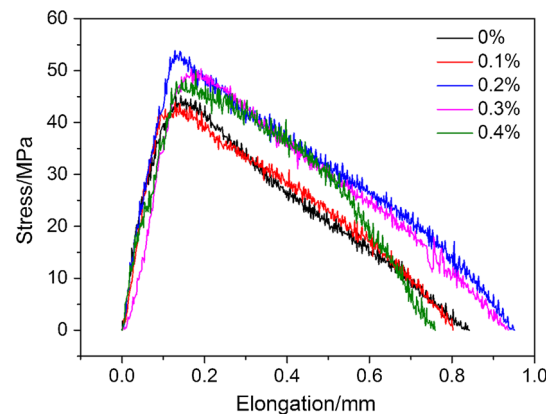


**Fig. 9** Stress–elongation curves as a function of BaTiO<sub>3</sub> content

### 3.2 Spreadability

The spreadability is an important indicator to evaluate the performance of lead-free solders in the electronic packaging. Figure 8 depicts the relationship between the BaTiO<sub>3</sub> content and the spreading coefficient of the SAC solder on the copper substrate, the spreading coefficient is increased firstly by adding the BaTiO<sub>3</sub> particle, the largest spreading coefficient (0.7836) is obtained in the SAC–0.2BaTiO<sub>3</sub> composite solder, it is 23.48 % higher than that of the SAC solder. The spreading coefficient is decreased with increasing the BaTiO<sub>3</sub> content in the SAC–(0.2–0.4)BaTiO<sub>3</sub> solders. It is demonstrated that the spreadability is improved by the small addition of BaTiO<sub>3</sub> particle in the SAC composite solder.

Similar results have been observed in Refs. [8, 19], and the results can be attributed to the diminished interfacial tension in the SAC–(0.2–0.4)BaTiO<sub>3</sub> solders. The interfacial tension between the liquid solder and the copper substrate is reduced due to the existence of the BaTiO<sub>3</sub>

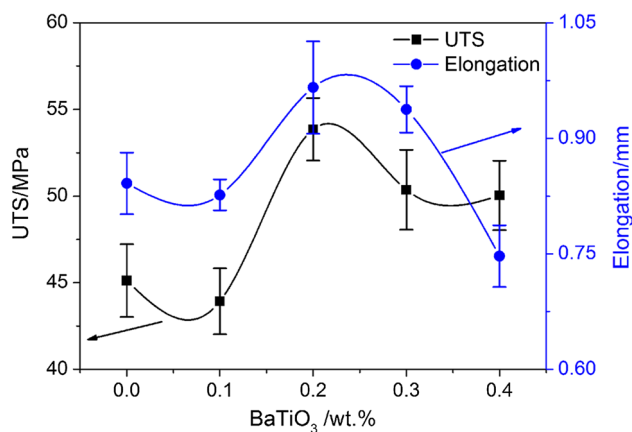


**Fig. 10** Effect of BaTiO<sub>3</sub> particle additions on UTS and elongation

**Table 2** UTS and elongation of the SAC composite solders

Alloy	UTS (MPa)	Elongation (mm)
SAC	45.12	0.84
SAC–0.1BaTiO <sub>3</sub>	43.92	0.82
SAC–0.2BaTiO <sub>3</sub>	53.85	0.96
SAC–0.3BaTiO <sub>3</sub>	50.36	0.93
SAC–0.4BaTiO <sub>3</sub>	50.03	0.74

particle, the fluidity of the liquid solder is increased on the Cu substrate due to the diminished interfacial tension. Consequently, the spreading coefficient is increased and the spreadability is improved. The BaTiO<sub>3</sub> particle is agglomerated and floated on the surface of the liquid solder with further increasing the BaTiO<sub>3</sub> addition, the fluidity of the liquid solder on the Cu substrate is decreased, and the spreadability is deteriorated finally.

### 3.3 Tensile property

Figure 9 reveals the stress–elongation curves of the SAC solder specimens. The stress is increased linearly and then is decreased slowly with increasing the elongation. The maximum stress values are in the range of 40–50 MPa, the elongation is approximately 0.15 mm, and the maximum elongations are exceed 0.7 mm. Figure 10 illustrates the relationship between the tensile property of the SAC solder and the BaTiO<sub>3</sub> particle content, the values of UTS and elongation are listed in Table 2. The maximum UTS (53.85 MPa) is obtained in the SAC + 0.2 wt% BaTiO<sub>3</sub> solder, it is 19 % higher than that of the SAC solder. The UTS is changed slightly in the SAC–(0.2–0.4)BaTiO<sub>3</sub> solders. As shown in Fig. 4c, the refined lamellar β-Sn is observed in the SAC–0.2BaTiO<sub>3</sub> solder. The greater tensile force is needed to promote the movement of dislocations compared with the coarsened block microstructure, and the better tensile property is obtained in the SAC–0.2BaTiO<sub>3</sub> solder.

### 3.4 Fracture surface analysis

The fracture surfaces of the SAC–0.2BaTiO<sub>3</sub> composite solder after tensile tests are presented in Fig. 11. The position of tensile fracture occurs in the middle of the solder joint according to the macroscopic fracture surface in Fig. 11a. A large number of homogeneous dimples are observed on the fracture surface in Fig. 11b, it is indicated that the tensile specimen worked in a highly ductile manner. The EDS results show that some minor Cu<sub>6</sub>Sn<sub>5</sub> IMC particles are detected at the bottom of the dimple signed with the black square frame in Fig. 11b. It is illustrated that the fracture position occurs in the internal solder/solder near the boundary of IMC.

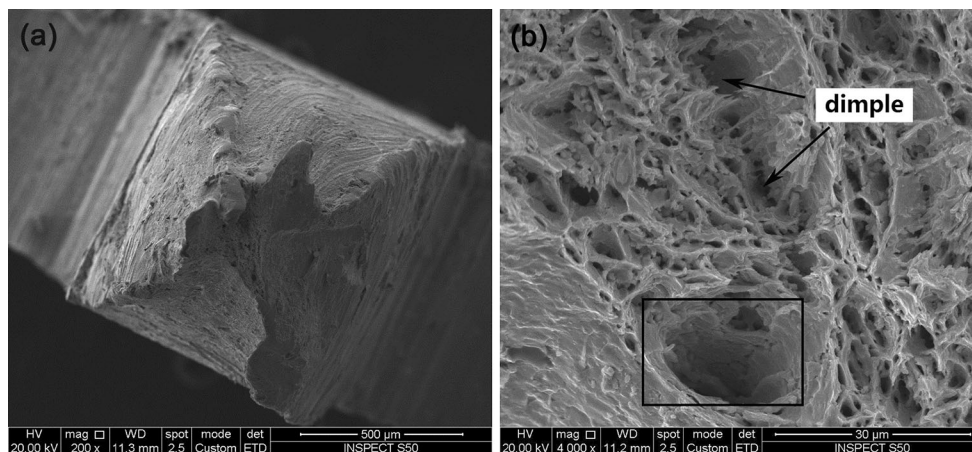


**Fig. 11** SEM micrographs showing the tensile fracture surfaces of SAC–0.2BaTiO<sub>3</sub>

## 4 Conclusions

1. The  $\beta$ -Sn is refined and the volume fraction of the eutectic phase is increased by adding BaTiO<sub>3</sub> particle. The  $\beta$ -Sn morphology is transformed from the block into the lamellar in the SAC + 0.2 wt% BaTiO<sub>3</sub> composite solder.
2. The thickness of the SAC–0.2BaTiO<sub>3</sub> composite solder reaches about 7.3  $\mu$ m that is twice thicker than that of the SAC solder, the IMC layer is identified as Cu<sub>6</sub>Sn<sub>5</sub>.
3. The largest spreading coefficient (0.7836) is obtained in the SAC–0.2BaTiO<sub>3</sub> composite solder. It exhibits the excellent solderability due to the diminished interfacial tension.
4. The UTS and the elongation are improved by adding 0.2 wt% BaTiO<sub>3</sub>. The fracture surface is uniformly consisted of large amounts of dimples due to the highly ductile manner.

**Acknowledgments** This research was financially supported by the National Natural Science Foundation of China (Grant No. 51401037), the Science and Technology Program of Jiangsu Province of China (Grant No. BK20141228), the Science and Technology Program of Suzhou (Grant Nos. SYG201421, SYG201348, and SYG201251), the Natural Science Foundation of the Jiangsu Higher Education Institutions of China (Grant Nos. 14KJB430001 and 13KJB430001), the Scientific Research Project of Changshu Institute of Technology (JXK2014003), and Jiangsu Key Laboratory of Large Engineering Equipment Detection and Control under Grant No. JSKLEDC201301.

## References

1. V.L. Niranjani, B.S.S.C. Rao, V. Singh, S.V. Kamat, Influence of temperature and strain rate on tensile properties of single walled carbon nanotubes reinforced Sn–Ag–Cu lead free solder alloy composites. *Mater. Sci. Eng. A* **529**, 257–264 (2011)
2. C.M.L. Wu, D.Q. Yu, C.M.T. Law, L. Wang, Properties of lead-free solder alloys with rare earth element additions. *Mater. Sci. Eng. R Rep.* **44**(1), 1–44 (2004)
3. J.B. Wan, Y.C. Liu, C. Wei, Z.M. Gao, C.S. Ma, Effect of Al content on the formation of intermetallic compounds in Sn–Ag–Zn lead-free solder. *J. Mater. Sci. Mater. Electron.* **19**(3), 247–253 (2010)
4. Choi Hyelim, Lee Tae-Kyu, Kim Yusung, Kwon Hoon, Tseng ChienFu, Duh Jenq Gong, Choe Heeman. Improved strength of boron-doped Sn–1.0Ag–0.5Cu solder joints under aging conditions. *Intermetallics* **20**(1), 155–159 (2012)
5. K. Zeng, K.N. Tu, Six cases of reliability study of Pb-free solder joints in electronic packaging technology. *Mater. Sci. Eng. R Rep.* **38**(2), 55–105 (2002)
6. A.A. El-Daly, A.E. Hammad, A. Fawzy, D.A. Nasrallah, Microstructure, mechanical properties, and deformation behavior of Sn–1.0Ag–0.5Cu solder after Ni and Sb additions. *Mater. Des.* **43**, 40–49 (2013)
7. Liang Zhang, Ji-guang Han, Cheng-wen He, Yong-huan Guo, Effect of Zn on properties and microstructure of SnAgCu alloy. *J. Mater. Sci. Mater. Electron.* **23**(11), 1950–1956 (2012)
8. X.D. Liu, Y.D. Han, H.Y. Jing, J. Wei, L.Y. Xu, Effect of graphene nanosheets reinforcement on the performance of Sn–Ag–Cu lead-free solder. *Mater. Sci. Eng. A* **562**, 25–32 (2013)
9. L.C. Tsao, S.Y. Chang, Effects of Nano-TiO<sub>2</sub> additions on thermal analysis, microstructure and tensile properties of Sn<sub>3.5</sub>Ag<sub>0.25</sub>Cu solder. *Mater. Des.* **31**(2), 990–993 (2010)
10. B.L. Chen, G.Y. Li, Influence of Sb on IMC growth in Sn–Ag–Cu–Sb–Pb-free solder joints in reflow process. *Thin Solid Films* **462–463**, 395–401 (2004)
11. Gao Feng, Cheng Fangjie, Nishikawa Hiroshi, Takemoto Tada-shi, Characterization of Co–Sn intermetallic compounds in Sn–3.0Ag–0.5Cu–0.5Co lead-free solder alloy. *Mater. Lett.* **62**(15), 2257–2259 (2008)
12. Moser Zbigniew, Sebo Pavol, Gasior Wladyslaw, Svec Peter, Pstrus Janusz, Effect of indium on wettability of Sn–Ag–Cu solders. Experiment vs. modeling, Part I. *Calphad* **33**(1), 63–68 (2009)
13. Y. Liu et al., Effect of Ni, Bi concentration on the microstructure and shear behavior of low-Ag SAC–Bi–Ni/Cu solder joints. *J. Mater. Sci. Mater. Electron.* **25**(6), 2627–2633 (2014)
14. T. Fouzder, I. Shafiq, Y.C. Chan, A. Sharif, W.K.C. Yung, Influence of SrTiO<sub>3</sub> nano-particle on the microstructure and shear strength of Sn–Ag–Cu solder on Au/Ni metallized Cu pads. *J. Alloys Compd.* **509**, 1885–1892 (2011)
15. L. Yang, C. Du, J. Dai, N. Zhang, Y. Jing, Effect of nanosized graphite on properties of Sn–Bi solder. *J. Mater. Sci. Mater. Electron.* **24**(11), 4180–4185 (2013)
16. L. Gao, S. Xue, L. Zhang, Z. Sheng, G. Zeng, F. Ji, Effects of trace rare earth Nd addition on microstructure and properties of SnAgCu solder. *J. Mater. Sci. Mater. Electron.* **21**(7), 643–648 (2009)
17. X. Wang, Y.C. Liu, C. Wei, H.X. Gao, P. Jiang, L.M. Yu, Strengthening mechanism of SiC-particulate reinforced Sn–3.7Ag–0.9Zn lead-free solder. *J. Alloys Compd.* **480**, 662–665 (2009)
18. Toshinori Taishi, Yutaka Ohno, Ichiro Yonenaga, Constitutional supercooling in heavily As-doped Czochralski Si crystal growth. *J. Cryst. Growth* **393**, 42–44 (2014)
19. Wei Zhang, Ying Zhong, Chunqing Wang, Effects of diamond additions on wettability and distribution of SnAgCu composite solders. *J. Mater. Sci. Technol.* **28**(7), 661–665 (2012)